

Characterization of Spin-Orbit Effects in Superconductors In_5Bi_3 and In_5Sb_3

Yao Wei,^{1,2} Siyu Chen,^{1,3} and Bartomeu Monserrat^{1,3,*}

¹*Department of Materials Science and Metallurgy, University of Cambridge, 27 Charles Babbage Road, Cambridge CB3 0FS, United Kingdom*

²*Theory and Simulation of Condensed Matter (TSCM), King's College London, Strand, London WC2R 2LS, United Kingdom*

³*TCM Group, Cavendish Laboratory, University of Cambridge, J. J. Thomson Avenue, Cambridge CB3 0HE, United Kingdom*

We report a first principles computational analysis of two phonon-mediated superconductors, In_5Bi_3 and In_5Sb_3 . We show that spin-orbit coupling leads to splitting of electron bands around the Fermi energy, resulting in a suppression of the electronic density of states in both compounds. In In_5Bi_3 , the spin-orbit coupling is essential for the dynamical stability of the experimentally observed phase, and the calculated superconducting critical temperature is in close agreement with measurements. In In_5Sb_3 , the spin-orbit coupling significantly reduces the calculated superconducting critical temperature compared to calculations neglecting relativistic effects. Our work emphasises the subtle interplay between spin-orbit interactions and phonon-mediated superconductivity.

I. INTRODUCTION

Over the past century, significant advances in superconductivity research have set the stage for revolutionary applications across diverse sectors. Superconductors are pivotal in magnetic resonance imaging for medical diagnostics [1], could facilitate lossless power transmission in electrical grids [2], and revolutionise the computational paradigm with quantum computers [3]. Each of these applications underscores the transformative potential of superconductors in shaping modern technology and infrastructure. However, the lack of a superconductor at ambient conditions severely limits their actual impact.

The development of accurate microscopic theories of superconductivity, together with practical computational frameworks for the evaluation of superconducting critical temperatures, could aid in the search for a superconductor at ambient conditions. Recent progress in modelling techniques and computational capabilities have shed light on various quantum phenomena occurring within superconductor systems [4]. These developments are gradually bridging the experiment-theory gap, refining theoretical models that are becoming increasingly predictive.

In this work, we describe a comparative computational study of two superconductors, In_5Bi_3 and In_5Sb_3 , which have the same crystal structure but different electronic properties. In particular, bismuth exhibits stronger spin-orbit coupling compared to antimony, and we aim to explore the interplay between spin-orbit coupling and superconductivity in these materials.

The initial discovery of In_5Bi_3 , dating back to the 1960s [5–7] revealed a critical superconducting transition temperature of 4.2 K. Subsequent research used a variety of techniques to further characterize superconducting and other properties of In_5Bi_3 [8–11]. Compared with In_5Bi_3 , In_5Sb_3 has received less attention from the sci-

entific community [12–15]. Specifically, research on the superconductivity properties of In_5Sb_3 is limited to two papers from the 1980s, which report a critical superconducting transition temperature of 5.6 K [12, 13].

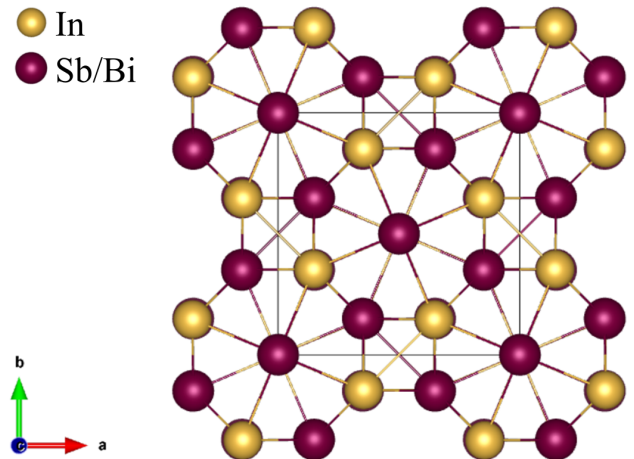


FIG. 1. Conventional unit cell of In_5Sb_3 as reported in entry 640434 of the Inorganic Crystal Structure Database (ICSD) [16]. Similarly, the conventional cell of In_5Bi_3 is also categorized according to entry 1244 of the ICSD. Both compounds share the same crystallographic space group $I4/mcm$ (140) as illustrated in this figure.

In this work, we describe first principles calculations combined with the Migdal-Eliashberg (ME) theory [17, 18] to study the superconducting properties of In_5Bi_3 and In_5Sb_3 , with a particular emphasis on the role of spin-orbit coupling (SOC). Regarding In_5Bi_3 , our calculations confirm the recent proposal that the inclusion of SOC plays a pivotal role in the structural stability of the material, and our predicted superconducting critical temperature is in close agreement with experimental values. For In_5Sb_3 , our phonon calculations show that the structural stability of the material does not depend

* bm418@cam.ac.uk

on spin-orbit coupling, but the calculated superconducting transition temperature is significantly influenced by spin-orbit coupling effects.

II. METHODS

A. Structure

We investigate the physical properties of In_5Bi_3 and In_5Sb_3 starting from the experimentally determined crystal structures. Both In_5Bi_3 and In_5Sb_3 have a tetragonal crystal structure with $I4/mcm$ space group (No. 140) and 16 atoms in the primitive cell, as is shown in Fig. 1. In_5Bi_3 has lattice parameters of $a = 8.484 \text{ \AA}$ and $c = 12.590 \text{ \AA}$ [12] and In_5Sb_3 has lattice parameters of $a = 8.340 \text{ \AA}$ and $c = 12.340 \text{ \AA}$ [19].

B. Computational methods

1. Electronic structure calculations and geometry optimization

We perform first principles calculations using density functional theory [20, 21] with QUANTUM ESPRESSO [22, 23]. The generalized gradient approximation of Perdew-Burke-Ernzerhof (PBE) is used to approximate the exchange-correlation functional [24]. We use ultrasoft pseudopotentials [25] (pbe-kjpaw-psl) taken from the QUANTUM ESPRESSO pseudopotential library generated by Dal Corso [26]. The valence electrons are from the following atomic shells: indium $4d^{10}5s^25p^1$, bismuth $5d^{10}6s^26p^3$, and antimony $5s^25p^3$. After convergence tests, we choose a kinetic energy cutoff of 60 Ry, and a Monkhorst-Pack \mathbf{k} -point grid of size $6 \times 6 \times 6$ for both In_5Bi_3 and In_5Sb_3 . Moreover, when the total energy change between two consecutive self-consistent iterations is less than 2×10^{-9} Ry, the calculation is considered as converged. We report calculations both with and without the spin-orbit coupling (SOC) [27]. The ionic relaxation is considered complete if atomic forces are less than 10^{-10} Ry/bohr, and we keep the cell parameters fixed to their experimental values.

2. Phonons and electron-phonon coupling

We calculate phonons using density functional perturbation theory (DFPT) as implemented in QUANTUM ESPRESSO [22, 28]. We use a coarse $4 \times 4 \times 4$ phonon \mathbf{q} -point grid to evaluate the force constants, and then use Fourier interpolation of the dynamical matrices onto a finer grid to evaluate the phonon dispersion.

For the electron-phonon coupling calculations, we employ a $6 \times 6 \times 6$ electron \mathbf{k} -point grid and a $4 \times 4 \times 4$ phonon \mathbf{q} -point grid to compute the electron-phonon matrix elements in QUANTUM ESPRESSO [22, 28]. Subsequently,

we used the WANNIER90 package [29, 30] and the EPW package [31–33] to interpolate the electron-phonon coupling (EPC) constants onto coarse $8 \times 8 \times 8$ \mathbf{k} -point and $4 \times 4 \times 4$ \mathbf{q} -point meshes, as well as onto finer $24 \times 24 \times 24$ \mathbf{k} -point and $8 \times 8 \times 8$ \mathbf{q} -point meshes. The initial guess for the projections on localized orbitals using WANNIER90 is detailed in the Supporting Information.

3. Superconducting transition temperature

We evaluate the superconducting critical temperature T_c using the Allen-Dynes formula [34, 35]:

$$T_c = \frac{\omega_{\log}}{1.2} \exp\left(-\frac{1.04(1+\lambda)}{\lambda - \mu^*(1+0.62\lambda)}\right), \quad (1)$$

where $\omega_{\log} = \exp\left[\frac{2}{\lambda} \int \frac{d\omega}{\omega} \alpha^2 F(\omega) \log \omega\right]$ is a logarithmic average of the phonon frequencies [36, 37], μ^* is the screened Coulomb potential that we treat as an empirical parameter [32], $\lambda = 2 \int_0^\infty \frac{\alpha^2 F(\omega)}{\omega} d\omega$ is the electron-phonon coupling constant, and $\alpha^2 F(\omega)$ is the Eliashberg spectral function. The spectral function is given by [34, 38]:

$$\alpha^2 F(\omega) = \frac{1}{2\pi N(\epsilon_F)} \sum_{\mathbf{q}\nu} \delta(\omega - \omega_{\mathbf{q}\nu}) \frac{\gamma_{\mathbf{q}\nu}}{\hbar\omega_{\mathbf{q}\nu}}, \quad (2)$$

where $N(\epsilon_F)$ is the electronic density of states at the Fermi level, $\omega_{\mathbf{q}\nu}$ is the frequency of the phonon with wave vector \mathbf{q} and branch label ν , and $\gamma_{\mathbf{q}\nu}$ is the associated phonon linewidth arising from electron-phonon coupling. In turn, the linewidth is given by [34, 38]:

$$\gamma_{\mathbf{q}\nu} = \frac{2\pi\omega_{\mathbf{q}\nu}}{\Omega_{\text{BZ}}} \sum_{ij} \int d^3k \left| g_{\mathbf{k},\mathbf{q}\nu}^{ij} \right|^2 \delta(\epsilon_{\mathbf{k},i} - \epsilon_F) \delta(\epsilon_{\mathbf{k}+\mathbf{q},j} - \epsilon_F), \quad (3)$$

where $\epsilon_{\mathbf{k},i}$ is the electronic energy for band i and wave vector \mathbf{k} , Ω_{BZ} is the volume of the Brillouin zone, and $g_{\mathbf{k},\mathbf{q}\nu}^{ij}$ is the electron-phonon interaction matrix element. Finally, the electron-phonon matrix element is given by:

$$g_{\mathbf{k},\mathbf{q}\nu}^{ij} = \left(\frac{\hbar}{2M\omega_{\mathbf{q}\nu}} \right)^{1/2} \langle \psi_{i\mathbf{k}+\mathbf{q}} | \partial_{\mathbf{q}\nu} V | \psi_{j\mathbf{k}} \rangle, \quad (4)$$

where M is the mass of the atoms, $\psi_{i\mathbf{k}+\mathbf{q}}$ and $\psi_{j\mathbf{k}}$ represent the Bloch wavefunctions of the electronic states involved in the coupling, and $\partial_{\mathbf{q}\nu} V$ denotes the derivative of the crystal potential with respect to the $\mathbf{q}\nu$ phonon displacement.

We also estimated T_c by solving the Eliashberg equations [32, 39, 40]:

$$Z(i\omega_n) = 1 + \frac{\pi T}{\omega_n} \sum_{n'} \frac{\omega_{n'}}{\sqrt{R(i\omega_{n'})}} \lambda(n - n'), \quad (5)$$

$$Z(i\omega_n) \Delta(i\omega_n) = \pi T \sum_{n'} \frac{\Delta(i\omega_{n'})}{\sqrt{R(i\omega_{n'})}} [\lambda(n - n') - \mu^*], \quad (6)$$

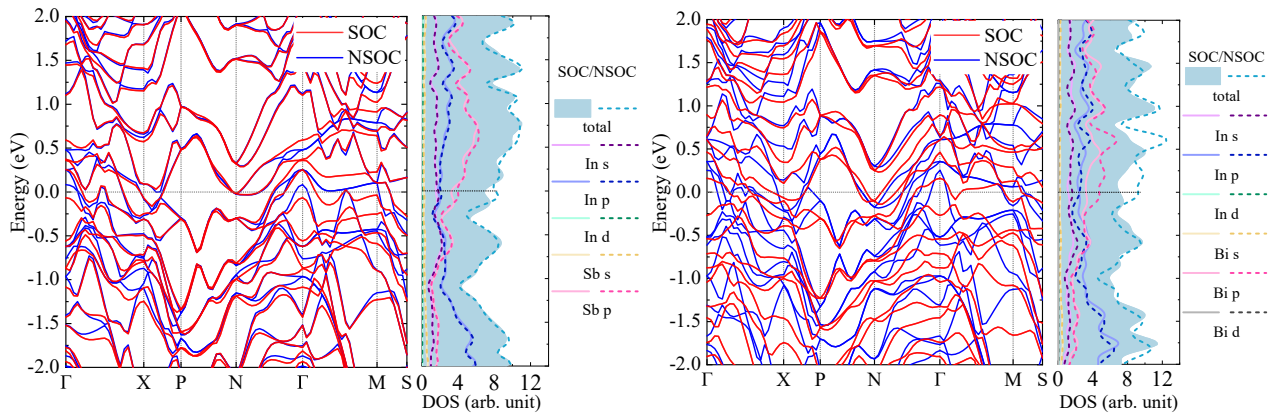


FIG. 2. Electronic band structure (left) and projected Density of States (DOS, right) of In_5Sb_3 (left panel) and In_5Bi_3 (right panel). The results of non-spin-orbit coupling(NSOC) are shown by blue lines, while with SOC by red lines. Atom-projected DOS, as well as projections onto s , p , d orbitals of In are shown in purple, blue, and green, whereas projections on s orbit of Sb/Bi, p orbit of Sb/Bi, d orbit of Bi are shown in yellow, pink and grey, respectively. The zero of the energy is chosen at the Fermi level.

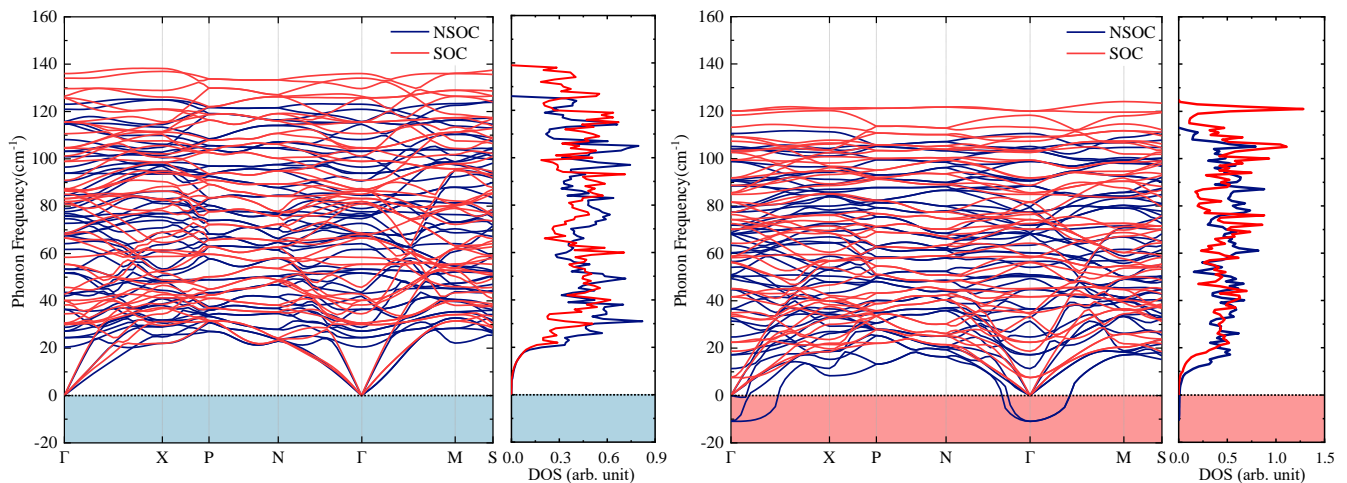


FIG. 3. Phonon dispersion (left) and phonon DOS (right) of In_5Sb_3 (left panel) and In_5Bi_3 (right panel). The results with and without SOC are shown by red and dark blue lines, respectively.

where $R(i\omega_{n'})$ and $\lambda(n - n')$ are given by:

$$R(i\omega_n) = \omega_n^2 + \Delta^2(i\omega_n), \quad (7)$$

$$\lambda(n - n') = \int_0^\infty d\omega \frac{2\omega\alpha^2 F(\omega)}{(\omega_n - \omega_{n'})^2 + \omega^2}, \quad (8)$$

and where ω_n stands for the Matsubara frequency, and Z and Δ represent the renormalization function and the superconducting gap, respectively.

III. RESULTS AND DISCUSSION

A. Electronic properties

We present the electronic band structure and the atom-projected density of states (PDOS) with and without SOC for both In_5Sb_3 and In_5Bi_3 in Fig. 2. Both compounds exhibit metallic band structures with similar band dispersions.

The effects of SOC on the band structure are more pronounced in In_5Bi_3 , which is expected from the larger spin-orbit coupling effect of the heavier bismuth compared to that of antimony. Indeed, the SOC electronic structure of In_5Bi_3 exhibits an important reduction in the density of states near the Fermi level compared to the non-SOC counterpart, a feature that has been shown

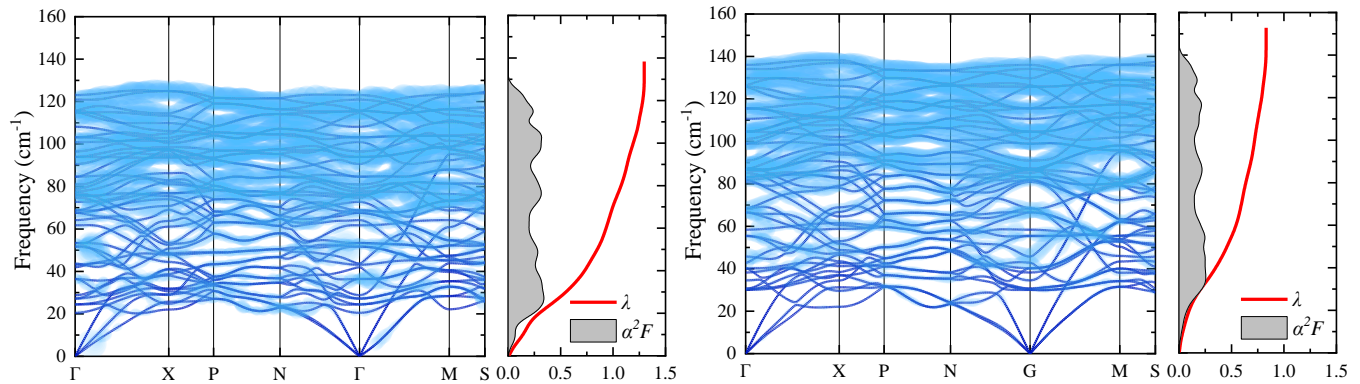


FIG. 4. Phonon linewidth, the width of the lines is proportional to their intrinsic linewidth (left) and Eliashberg function α^2F and accumulated EPC coefficient λ (right) for In_5Sb_3 (left panel) without SOC and (right panel) with SOC.

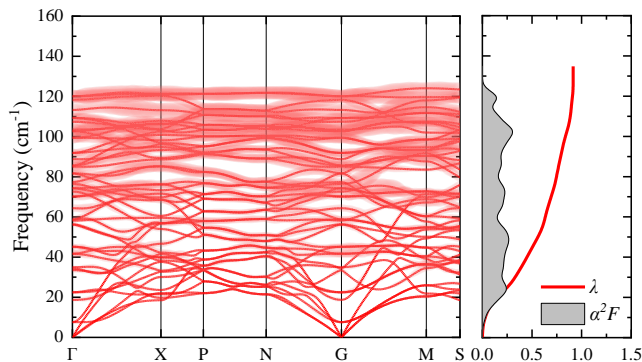


FIG. 5. Phonon linewidth, the width of the lines is proportional to their intrinsic linewidth (left) and Eliashberg function α^2F and accumulated EPC coefficient λ (right) for In_5Bi_3 with SOC.

to be key in determining the structural stability of this compound [41]. Our PDOS results clarify that the main disparity between calculations of In_5Bi_3 with and without SOC originates from the distinct p-orbital characteristics of bismuth.

B. Phonon properties

The calculated phonon spectra and phonon DOS for In_5Sb_3 and In_5Bi_3 , with and without SOC, are shown in Fig. 3. In_5Sb_3 is dynamically stable irrespective of whether SOC is included or not. The inclusion of SOC causes an upward shift in phonon frequencies across the spectrum, with the highest frequency obtained with SOC surpassing the non-SOC counterpart by 15 cm^{-1} .

In_5Bi_3 exhibits an imaginary frequency phonon mode centered around the Γ point, when the calculation is performed without the SOC, but the phonon frequencies become real with the inclusion of the SOC. This finding is consistent with the results reported in Ref. [41], and indi-

cates that the dynamical stability of In_5Bi_3 requires the inclusion of the spin-orbit coupling. We note that the highest phonon frequency in the present calculations is higher in the SOC-inclusive case compared to those conducted without SOC, which is an opposite trend to that reported previously [41]. This discrepancy likely arises from differences in the first principles implementations used, including different pseudopotentials and different treatment of the spin-orbit interaction.

A comparison of the phonon dispersions of In_5Sb_3 and In_5Bi_3 shows that the phonon frequencies for In_5Sb_3 exhibit higher values than those of In_5Bi_3 , as expected from the smaller mass of antimony compared to bismuth.

C. Electron-phonon coupling

1. Linewidth

Figures 4 and 5 show the calculated electron-phonon coupling linewidth, Eliashberg function α^2F and cumulative EPC coefficient λ for In_5Sb_3 and In_5Bi_3 .

In Fig. 4(a), the phonon dispersion and phonon linewidth of In_5Sb_3 without the SOC are presented. It can be observed that in regions where the phonon frequencies are higher, the linewidth tends to be larger as well. Figure 4(b) gives the phonon dispersion and phonon linewidth for In_5Sb_3 with SOC included. As previously mentioned, the phonon dispersion exhibits higher frequencies in the presence of SOC compared to the one without SOC. Despite the changes in the dispersion, the phonon linewidth maintains a strikingly similar trend when SOC is introduced. This observation indicates that the effect of SOC on the phonon linewidth is minimal, with only a $1.05 \times 10^{-2} \text{ meV}$ difference in the maximum phonon linewidth observed between the two cases with and without SOC. This finding might be significant as it suggests that, at least in the context of In_5Sb_3 , the inclusion of the spin-orbit coupling has

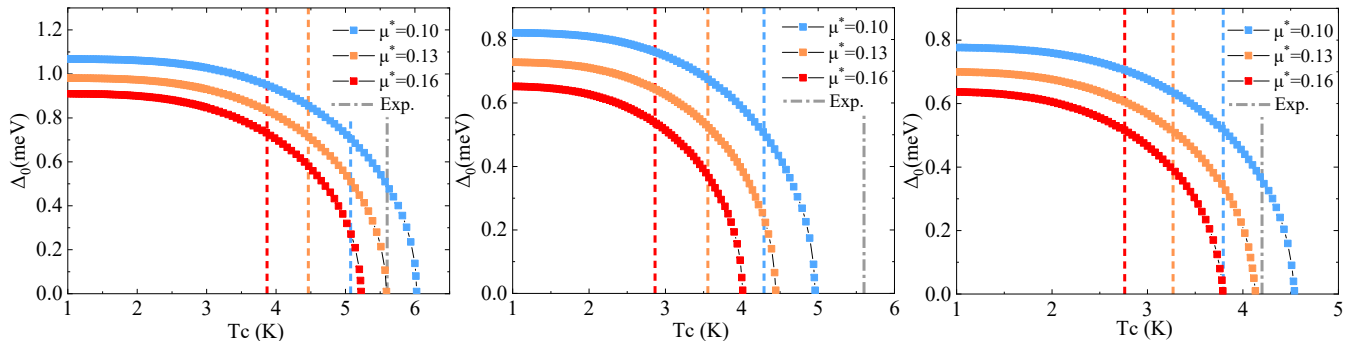


FIG. 6. The isotropic gap of stable In_5Sb_3 and In_5Bi_3 as a function of temperature: (a) In_5Sb_3 without SOC, (b) In_5Sb_3 with SOC and (c) In_5Bi_3 with SOC. The dashed vertical lines show the T_c via the McMillan equation with μ^* taken as 0.16, 0.13 and 0.10, respectively.

a more pronounced effect on phonon frequencies rather than on phonon linewidth.

In the case of In_5Bi_3 the phonon spectrum without SOC contains imaginary frequencies and hence only results with the SOC included have physical significance. Figure 5 shows the phonon dispersion and phonon linewidth characteristics for In_5Bi_3 with SOC. It reveals a distinct behaviour compared to the case of the In_5Sb_3 system: the phonon linewidth of In_5Bi_3 is lower than the corresponding value in In_5Sb_3 under the same SOC conditions. The reason lies in the greater atomic mass of bismuth in comparison to antimony. This results in a diminished elastic force between atoms, subsequently leading to a weaker electron-phonon interaction and a reduced value of the phonon linewidth for In_5Bi_3 .

2. Superconducting transition temperature

In Fig. 6, the isotropic gaps of In_5Sb_3 and In_5Bi_3 are shown as a function of temperature. These results are obtained by solving the Eliashberg equations for each temperature while considering a few typical values of the effective screened Coulomb repulsion constant μ^* in the range of 0.1-0.16 [37]. Additionally, the McMillan equation is used to estimate the superconducting critical temperature for comparison.

Figure 6(a) displays the T_c prediction for In_5Sb_3 without SOC. At 0 K, the gap is observed with isotropic characteristics, and the energy of this gap spreads ranging from 0.9 to 1.1 meV when μ^* takes values from 0.10 to 0.16, the gap vanishes at 5.2 – 6.0 K, which is identified as the T_c from our calculation. Furthermore, the T_c was also estimated using the Allen-Dynes modified McMillan equation, with the same μ^* values from 0.10 to 0.16. The calculated T_c values are from 3.87 K to 5.07 K; these predictions are lower than the T_c values obtained from the Eliashberg equations.

In Fig. 6(b), we investigate the impact of SOC on the superconducting transition temperature of In_5Sb_3 . The

inclusion of SOC leads to a reduction in the predicted T_c when compared to the scenario without SOC shown in panel (a). At 0 K, the energy range of the superconducting gap spans from 0.65 to 0.81 meV. Under the influence of SOC, the critical temperature, which signifies the onset of superconductivity, is estimated to be approximately 4.94 K, 4.48 K and 3.98 K when μ^* takes values of 0.10, 0.13 and 0.16, respectively, as calculated using the Eliashberg equations. Furthermore, alternative calculations utilizing the Allen-Dynes modified McMillan equation produce T_c predictions of 4.29 K, 3.56 K and 2.86 K when μ^* is equal to 0.10, 0.13 and 0.16, respectively.

Comparing the results obtained with and without SOC for In_5Sb_3 , we observed a higher superconducting transition temperature in the non-SOC case. This trend can be attributed to a reduction in the electronic density of states at the Fermi level, particularly in the antimony p orbitals, upon including SOC. This reduction may be a general phenomenon, as SOC typically lifts band degeneracies, which can reduce the electronic density of states near the Fermi level.

As illustrated in Fig. 3, In_5Bi_3 exhibits imaginary frequencies in the absence of SOC, so it is not meaningful to discuss the T_c under these conditions. Instead, we can perform a calculation in the presence of SOC, and in Fig. 6(c) the dependence of the gap on temperature and the calculated values of T_c for In_5Bi_3 for a range of μ^* values are shown. Predictions of T_c closely resemble those of In_5Sb_3 with the inclusion of SOC when both the modified Allen-Dynes McMillan equation and the Eliashberg equation are used. Using the Eliashberg equation, T_c is estimated to be approximately 4.51 K, 4.14 K and 3.78 K when μ^* is set to 0.10, 0.13 and 0.16, respectively. Alternative calculations utilizing the Allen-Dynes modified McMillan equation produce T_c predictions of 3.79 K, 3.27 K and 2.76 K when μ^* is set to 0.10, 0.13 and 0.16, respectively, which somewhat underestimates the value from Eliashberg equation.

Notably, the experimental data reported in a previous study [41] recorded a T_c of approximately 4.2 K for In_5Bi_3

which falls within the predicted range and is closest to the value we obtain with $\mu^* = 0.13$. This agreement between theoretical calculations and experiments can be considered excellent. In contrast, earlier experimental studies [12] have reported a superconducting transition temperature for In_5Sb_3 in the range of approximately 5.0-5.6 K. Our predictions under spin-orbit SOC conditions fall short of this experimentally observed range. It is also noteworthy that this measurement was documented only once, nearly forty years ago.

IV. CONCLUSIONS

In summary, our investigation into the electronic and phonon properties of In_5Sb_3 and In_5Bi_3 has provided valuable insights into their superconducting behaviour and the impact of the spin-orbit coupling on their electronic and phonon structures and on their superconducting properties. Our analysis demonstrates that spin-orbit coupling can exert a significant influence on these properties, leading to shifts in phonon frequencies and superconducting transition temperatures. Specifically, we find that the inclusion of spin-orbit coupling reduces the electronic density of states near the Fermi energy, which drives the structural stabilisation of In_5Bi_3 and suppresses the superconducting critical temperature in In_5Sb_3 . These results highlight the importance of accounting for spin-orbit coupling in predictive models, as it can have a substantial impact on the physical properties of materials containing heavy elements.

The theoretical predictions for the critical temperature of In_5Bi_3 demonstrate a close alignment with experimental results, which underscores the validity of our theoretical framework for explaining the superconducting characteristics of such materials. The predicted superconducting temperature of In_5Sb_3 somewhat underestimates the experimentally reported value, but the latter has only been reported once decades ago, so it may be interesting to revisit the superconducting properties of In_5Sb_3 experimentally.

ACKNOWLEDGMENTS

Y.W. gratefully acknowledges funding from the China Scholarship Council. S.C. acknowledges financial support from the Cambridge Trust and from the Winton Programme for the Physics of Sustainability. B.M. acknowledges support from a UKRI Future Leaders Fellowship (MR/V023926/1), from the Gianna Angelopoulos Programme for Science, Technology, and Innovation, and from the Winton Programme for the Physics of Sustainability. Computational resources were provided through our membership in the UK's HEC Materials Chemistry Consortium, funded by EPSRC (EP/R029431 and EP/X035859). This work utilized ARCHER2, the UK National Supercomputing Service (<http://www.archer2.ac.uk>), as well as resources from the UK Materials and Molecular Modelling Hub (MMM Hub), which is partially supported by EPSRC (EP/T022213 and EP/W032260).

-
- [1] Yuri Lvovsky, Ernst Wolfgang Stautner, and Tao Zhang, “Novel technologies and configurations of superconducting magnets for mri,” *Superconductor Science and Technology* **26**, 093001 (2013).
 - [2] AP Malozemoff, “Electric power grid application requirements for superconductors,” *MRS bulletin* **36**, 601–607 (2011).
 - [3] Karl K Berggren, “Quantum computing with superconductors,” *Proceedings of the IEEE* **92**, 1630–1638 (2004).
 - [4] Erik Van Der Giessen, Peter A Schultz, Nicolas Bertin, Vasily V Bulatov, Wei Cai, Gábor Csányi, Stephen M Foiles, Marc GD Geers, Carlos González, Markus Hütter, *et al.*, “Roadmap on multiscale materials modeling,” *Modelling and Simulation in Materials Science and Engineering* **28**, 043001 (2020).
 - [5] R Wang and NJ GRANT, “The crystal structure of in_5bi_3 ,” *Zeitschrift für Kristallographie-Crystalline Materials* **129**, 244–251 (1969).
 - [6] E Cruceanu, E Hering, and H Schwarz, “Electrical conductivity and superconductivity in in_5bi_3 ,” *Physics Letters A* **32**, 295–296 (1970).
 - [7] E Hering and E Cruceanu, “Hall effect in the mixed state of intrinsic type-ii-superconductor in_5bi_3 ,” *Physics Letters A* **38**, 431–432 (1972).
 - [8] SG Fries, JAH da Jornada, and A Maciel, “Experimental study of the electric field gradient in in_5bi_3 ,” *physica status solidi (a)* **74**, 661–666 (1982).
 - [9] LMW Schreurs and HM Weijers, “The in_5bi_3 phase in the in-bi system,” *Journal of crystal growth* **71**, 155–162 (1985).
 - [10] P Böttcher, Th Doert, Ch Druska, and S Bradtmöller, “Investigations on compounds with cr_5b_3 and in_5bi_3 structure types,” *Journal of alloys and compounds* **246**, 209–215 (1997).
 - [11] Olga Degtyareva and Valentina F Degtyareva, “Structural transformations in the in_5bi_3 compound under high pressure,” *Journal of Physics: Condensed Matter* **14**, 407 (2001).
 - [12] VF Degtyareva, SA Ivakhnenko, EG Ponyatovskii, and VI Rashchupkin, “Crystal structure and superconductivity of indium-rich in-bi and in-sb alloys after high-pressure treatment,” *Sov. Phys.-Solid State (Engl. Transl.);(United States)* **23** (1981).
 - [13] VF Degtyareva, IT Belash, GV Chipenko, EG Ponyatovskii, and VI Rashchupkin, “Intermediate phases obtained by applying high pressure to the in-sb system,” *Sov. Phys.-Solid State (Engl. Transl.);(United States)* **25** (1983).

- [14] RC Sharma, TL Ngai, and YA Chang, “The in-sb (indium-antimony) system,” *Bulletin of Alloy Phase Diagrams* **10**, 657–664 (1989).
- [15] NV Chandra Shekar, K Takemura, and H Yusa, “Synthesis experiments on in-sb and b-sb systems in a laser heated diamond-anvil cell,” *International Journal of High Pressure Research* **15**, 393–398 (1997).
- [16] Mariette Hellenbrandt, “The inorganic crystal structure database (icsd)—present and future,” *Crystallography Reviews* **10**, 17–22 (2004).
- [17] AB Migdal, “Interaction between electrons and lattice vibrations in a normal metal,” *Sov. Phys. JETP* **7**, 996–1001 (1958).
- [18] GM Eliashberg, “Interactions between electrons and lattice vibrations in a superconductor,” *Sov. Phys. JETP* **11**, 696–702 (1960).
- [19] R Kubiak, “Röntgenographische untersuchungen der intermetallischen phasen in5bi3, in2bi und inbi zwischen+ 60 und- 135 c,” *Zeitschrift für anorganische und allgemeine Chemie* **431**, 261–267 (1977).
- [20] Walter Kohn and Lu Jeu Sham, “Self-consistent equations including exchange and correlation effects,” *Physical review* **140**, A1133 (1965).
- [21] Pierre Hohenberg and Walter Kohn, “Inhomogeneous electron gas,” *Physical review* **136**, B864 (1964).
- [22] Paolo Giannozzi, Stefano Baroni, Nicola Bonini, Matteo Calandra, Roberto Car, Carlo Cavazzoni, Davide Ceresoli, Guido L Chiarotti, Matteo Cococcioni, Ismaila Dabo, *et al.*, “Quantum espresso: a modular and open-source software project for quantum simulations of materials,” *Journal of physics: Condensed matter* **21**, 395502 (2009).
- [23] Paolo Giannozzi, Oliviero Andreussi, Thomas Brumme, Oana Bunau, M Buongiorno Nardelli, Matteo Calandra, Roberto Car, Carlo Cavazzoni, Davide Ceresoli, Matteo Cococcioni, *et al.*, “Advanced capabilities for materials modelling with quantum espresso,” *Journal of physics: Condensed matter* **29**, 465901 (2017).
- [24] John P Perdew, Kieron Burke, and Matthias Ernzerhof, “Generalized gradient approximation made simple,” *Physical review letters* **77**, 3865 (1996).
- [25] David Vanderbilt, “Soft self-consistent pseudopotentials in a generalized eigenvalue formalism,” *Physical review B* **41**, 7892 (1990).
- [26] Andrea Dal Corso, “Pseudopotentials periodic table: From h to pu,” *Computational Materials Science* **95**, 337–350 (2014).
- [27] R Winkler, S Papadakis, E De Poortere, and M Shayegan, *Spin-orbit coupling in two-dimensional electron and hole systems*, Vol. 41 (Springer, 2003).
- [28] Stefano Baroni, Stefano De Gironcoli, Andrea Dal Corso, and Paolo Giannozzi, “Phonons and related crystal properties from density-functional perturbation theory,” *Reviews of modern Physics* **73**, 515 (2001).
- [29] Arash A Mostofi, Jonathan R Yates, Young-Su Lee, Ivo Souza, David Vanderbilt, and Nicola Marzari, “wannier90: A tool for obtaining maximally-localised wannier functions,” *Computer physics communications* **178**, 685–699 (2008).
- [30] Arash A Mostofi, Jonathan R Yates, Giovanni Pizzi, Young-Su Lee, Ivo Souza, David Vanderbilt, and Nicola Marzari, “An updated version of wannier90: A tool for obtaining maximally-localised wannier functions,” *Computer Physics Communications* **185**, 2309–2310 (2014).
- [31] Feliciano Giustino, Marvin L Cohen, and Steven G Louie, “Electron-phonon interaction using wannier functions,” *Physical Review B—Condensed Matter and Materials Physics* **76**, 165108 (2007).
- [32] Elena Roxana Margine and Feliciano Giustino, “Anisotropic migdal-eliasberg theory using wannier functions,” *Physical Review B* **87**, 024505 (2013).
- [33] Samuel Poncé, Elena R Margine, Carla Verdi, and Feliciano Giustino, “Epw: Electron–phonon coupling, transport and superconducting properties using maximally localized wannier functions,” *Computer Physics Communications* **209**, 116–133 (2016).
- [34] Ph B Allen and RC Dynes, “Transition temperature of strong-coupled superconductors reanalyzed,” *Physical Review B* **12**, 905 (1975).
- [35] RC Dynes, “Mcmillan’s equation and the tc of superconductors,” *Solid State Communications* **10**, 615–618 (1972).
- [36] CF Richardson and NW Ashcroft, “High temperature superconductivity in metallic hydrogen: Electron-electron enhancements,” *Physical review letters* **78**, 118 (1997).
- [37] Keun-Ho Lee, Kee-Joo Chang, and Marvin L Cohen, “First-principles calculations of the coulomb pseudopotential μ^* : Application to al,” *Physical Review B* **52**, 1425 (1995).
- [38] Philip B Allen, “Neutron spectroscopy of superconductors,” *Physical Review B* **6**, 2577 (1972).
- [39] Philip B Allen and Božidar Mitrović, “Theory of superconducting tc,” *Solid state physics* **37**, 1–92 (1983).
- [40] F Marsiglio, M Schossmann, and JP Carbotte, “Iterative analytic continuation of the electron self-energy to the real axis,” *Physical Review B* **37**, 4965 (1988).
- [41] Siyu Chen, Ryo Maezono, Jiasheng Chen, F Malte Grosche, Chris J Pickard, and Bartomeu Monserrat, “Chemical and structural stability of superconducting in5bi3 driven by spin–orbit coupling,” *Journal of Physics: Materials* **3**, 015007 (2019).

Characterization of Spin-Orbit Effects in Superconductors In_5Bi_3 and In_5Sb_3 Supporting Information

Yao Wei,^{1,2} Siyu Chen,^{1,3} and Bartomeu Monserrat^{1,3,*}

¹*Department of Materials Science and Metallurgy, University of Cambridge,
27 Charles Babbage Road, Cambridge CB3 0FS, United Kingdom*

²*Theory and Simulation of Condensed Matter (TSCM),
King's College London, Strand, London WC2R 2LS, United Kingdom*

³*TCM Group, Cavendish Laboratory, University of Cambridge,
J. J. Thomson Avenue, Cambridge CB3 0HE, United Kingdom*

arXiv:2410.20368v1 [cond-mat.supr-con] 27 Oct 2024

* bm418@cam.ac.uk

I. PSEUDOPOTENTIAL SELECTION

To explore the influence of the pseudopotential on the phonon dispersion within the QUANTUM ESPRESSO framework, we compare the calculations reported in the main text with those obtained using an alternative pseudopotential (pbe-dn-rrkjus-psl), and the results are depicted in Fig. 1. The observed trend closely resembles that described in the main text: without the SOC there are imaginary phonon frequencies which means that the crystal is dynamically unstable; including the SOC leads to real phonon frequencies and hence dynamical stability.

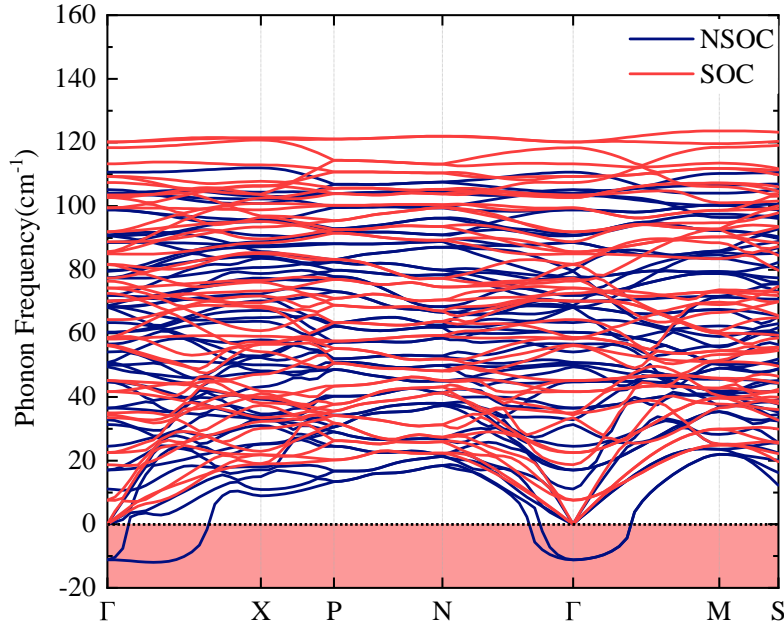


FIG. 1. Phonon dispersion of In_5Bi_3 . The results without SOC in dark blue lines and results with SOC in red lines to facilitate comparison, the pseudopotential is pbe-rrkjus-psl

II. WANNIER MODEL

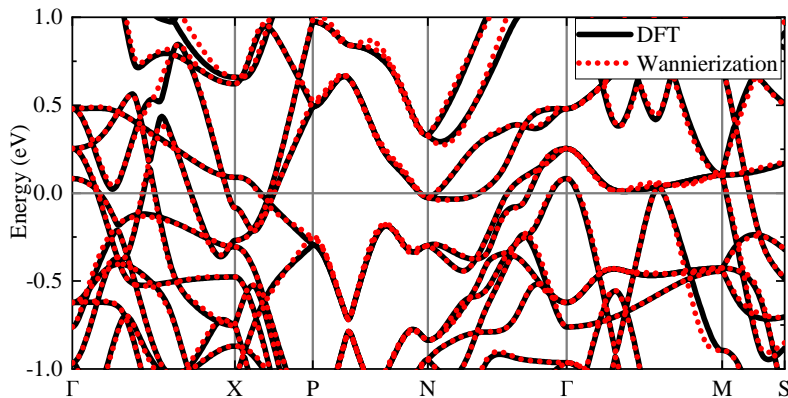


FIG. 2. The comparison of the electronic structure of In_5Sb_3 without SOC. The Fermi level is at 0.0 eV.

We use the WANNIER90 package [? ?] to construct Wannier orbitals from the Bloch states (Kohn-Sham orbitals) of the first principles calculations. We give an initial guess in the form of projections on localised orbitals onto Sb p and Bi p orbitals, and with 2 random orbitals in NSOC calculations, and 14 random orbitals in the SOC calculations. This

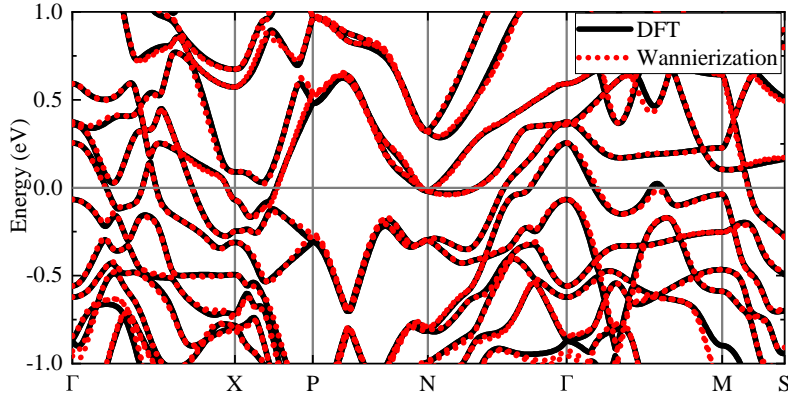


FIG. 3. The comparison of the electronic structure of In_5Sb_3 with SOC. The Fermi level is at 0.0 eV.

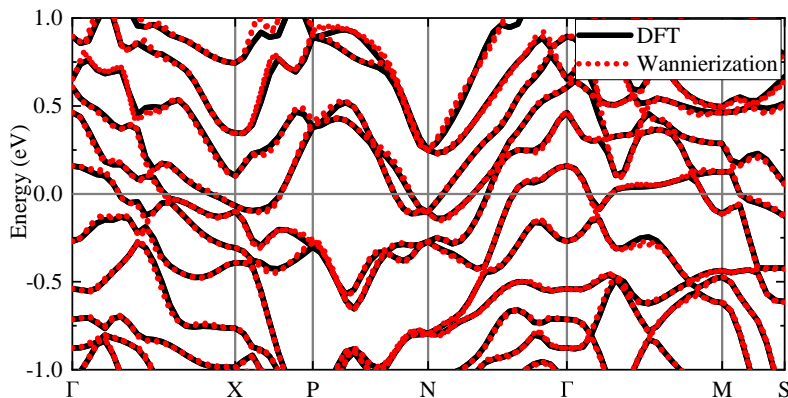


FIG. 4. The comparison of the electronic structure of In_5Bi_3 with SOC. The Fermi level is set to 0.0 eV.

procedure enables us to generate a tight-binding Hamiltonian with a basis of maximally localized Wannier functions [? ?], which leads to a band structure that closely resembles that obtained from DFT. A well-chosen Wannier window is essential for the accurate calculation of superconducting properties. The key parameters of Wannierization used in this study are presented in Tab. I.

Parameter	In_5Sb_3 NSOC	In_5Sb_3 SOC	In_5Bi_3 SOC
nbndsub	20	50	50
num_iter	3500	3500	3500
dis_froz_max	9.85	10.24	11.60
dis_froz_min	7.92	8.30	9.37
bands_skipped	exclude_bands = 1:65	exclude_bands = 1:112	exclude_bands = 1:160
proj(1)	random	random	random
proj(2)	Sb:p	Sb:p	Bi:p

TABLE I. The key parameters of Wannierization used in this study.

We compare the DFT band structure and the one obtained using Wannier orbitals and the tight-binding both with and without spin-orbit coupling. The results for In_5Sb_3 are shown in Figs. 2 and 3, while for In_5Bi_3 with SOC the results are shown in Fig. 4.

III. CONVERGENCE OF THE SUPERCONDUCTING TRANSITION TEMPERATURE

q -point grids	$2 \times 2 \times 2$	$3 \times 3 \times 3$	$4 \times 4 \times 4$
McMillan equation	1.90 K	4.02 K	4.46 K
Eliashberg equations	2.63 K	5.59 K	5.63 K

TABLE II. Predicted superconducting transition temperatures with different **q**-point grids for In_5Sb_3 without SOC, assuming $\mu^*=0.13$.

q -point grids	$2 \times 2 \times 2$	$3 \times 3 \times 3$	$4 \times 4 \times 4$
McMillan equation	0.76 K	2.85 K	3.27 K
Eliashberg equations	1.30 K	3.53 K	4.14 K

TABLE III. Predicted superconducting transition temperatures for In_5Bi_3 with SOC, calculated using different **q**-point grids, assuming $\mu^*=0.13$.

We compare the calculated superconducting transition temperatures for In_5Sb_3 without SOC, using **q**-point samplings of $2 \times 2 \times 2$, $3 \times 3 \times 3$, and $4 \times 4 \times 4$, as shown in Tab. II. For the $4 \times 4 \times 4$ **q**-point grid, the transition temperature is 5.63 K, determined using the Eliashberg equation. When using the $3 \times 3 \times 3$ grid, the temperature is only 0.04 K lower, indicating that the $3 \times 3 \times 3$ **q**-point sampling is sufficiently accurate for predicting the transition temperature in NSOC calculations. However, using the $2 \times 2 \times 2$ grid results in a T_c that is 2 K lower.

We also performed a comparison for In_5Bi_3 with SOC, using **q**-point grids of $2 \times 2 \times 2$, $3 \times 3 \times 3$, and $4 \times 4 \times 4$, as shown in Tab. III. For the $4 \times 4 \times 4$ grid, the transition temperature is approximately 0.6 K higher than for the $3 \times 3 \times 3$ grid, indicating that the electron-phonon coupling calculation has not yet converged at $3 \times 3 \times 3$ **q**-point sampling in SOC calculations. This highlights the need for higher precision in such calculations.